HHS Public Access

Author manuscript

Mol Cancer Ther. Author manuscript; available in PMC 2021 September 01.

Published in final edited form as:

Mol Cancer Ther. 2021 March ; 20(3): 553–563. doi:10.1158/1535-7163.MCT-20-0516.

Improved anti-Tumor Activity of the Fluoropyrimidine Polymer CF10 in pre-Clinical Colorectal Cancer Models thru Distinct Mechanistic and Pharmacological Properties

William H. Gmeiner[1,2,*], **Anthony Dominijanni**[3], **Alex O. Haber**[4], **Lais P. Ghiraldeli**[1], **David L. Caudell**[5], **Ralph D'Agostino Jr**[6], **Boris C. Pasche**[1,2], **Thomas L. Smith**[7], **Zhiyong Deng**[1], **Sezgin Kiren**[8], **Chinnadurai Mani**[9], **Komaraiah Palle**[9], **Jonathan R. Brody**[10]

[1]Department of Cancer Biology, Wake Forest School of Medicine, Winston-Salem, NC 27157 USA

[2]Comprehensive Cancer Center Wake Forest School of Medicine, Winston-Salem, NC 27157 USA

[3]Wake Forest Institute for Regenerative Medicine, Wake Forest School of Medicine, Winston-Salem, NC 27157 USA

[4]Department of Surgery, Jefferson Pancreas, Biliary and Related Cancer Center, Thomas Jefferson University, Philadelphia, PA 19107 USA

[5]Department of Pathology, Wake Forest School of Medicine, Winston-Salem, NC 27157 USA

[6]Department of Public Health Sciences, Wake Forest School of Medicine, Winston-Salem, NC 27157 USA

[7]Department of Orthopedic Surgery, Wake Forest School of Medicine, Winston-Salem, NC 27157 USA

[8]Department of Chemistry, Winston-Salem State University, Winston-Salem, NC 27110

[9]Department of Cell Biology and Biochemistry, Texas Tech University Health Sciences Centre, Lubbock, TX 79430 USA

[*] Corresponding Author: William H. Gmeiner, Wake Forest University School of Medicine, Medical Center Blvd, Winston-Salem, NC 27055. Phone: 336-716-6216; Fax: 336-716-0255; bgmeiner@wakehealth.edu.

Authors' Contributions

Conception and design: W.H. Gmeiner

Development of methodology:

Acquisition of data (provided animals, acquired and managed patients, provided facilities, etc.): A. Dominijanni, D. Caudell, L. Ghiraldeli, W.H. Gmeiner, A. Haber, C. Mani, T.L. Smith, C. Tracy, S. Kiren, Z. Deng

Analysis and interpretation of data (e.g. statistical analysis, biostatistics, computational analysis): J.R. Brody, D. Caudell, R. D'Agostino Jr, A. Dominijanni, W.H. Gmeiner, A. Haber, C. Mani, K. Palle

Writing, review, and/or revision of the manuscript: J.R. Brody, D. Caudell, R. D'Agostino Jr, A. Dominijanni, W.H. Gmeiner, A. Haber, C. Mani, K. Palle, B. Pasche, T.L. Smith.

Administrative, technical, or material support (i.e., reporting or organizing data, constructing databases):

Study Supervision: J.R. Brody, W.H. Gmeiner, K. Palle

Disclosure of Potential Conflicts of interest

W. Gmeiner is inventor on a patent application for CF10 in colon cancer.

[10]Brenden Colson Center for Pancreatic Care; Departments of Surgery and Cell, Developmental & Cancer Biology; Knight Cancer Institute, Oregon Health and Science University, Portland, OR 97239

Abstract

Chemotherapy regimens that include 5-fluorouracil (5-FU) are central to colorectal cancer (CRC) treatment, however risk/benefit concerns limit 5-FU's use, necessitating development of improved fluoropyrimidine (FP) drugs. In our study, we evaluated a 2nd generation nanoscale FP polymer, CF10, for improved anti-tumor activity. CF10 was more potent than the prototype FP polymer F10 and much more potent than 5-FU in multiple CRC cell lines including HCT-116, LS174T, SW480 and T84D. CF10 displayed improved stability to exonuclease degradation relative to F10 and reduced susceptibility to thymidine antagonism due to extension of the polymer with AraC. In CRC cells, CF10 strongly inhibited thymidylate synthase (TS), induced Top1 cleavage complex (Top1cc) formation and caused replication stress, while similar concentrations of 5-FU were ineffective. CF10 was well tolerated *in vivo* and invoked a reduced inflammatory response relative to 5-FU. Blood chemistry parameters in CF10 treated mice were within normal limits. In vivo, CF10 displayed anti-tumor activity in several CRC flank tumor models including HCT-116, HT-29, and CT-26. CF10's anti-tumor activity was associated with increased plasma levels of FP deoxynucleotide metabolites relative to 5-FU. CF10 significantly reduced tumor growth and improved survival (84.5 days vs 32 days; $p<0.0001$) relative to 5-FU in an orthotopic HCT-116-*luc* CRC model that spontaneously metastasized to liver. Improved survival in the orthotopic model correlated with localization of a fluorescent CF10 conjugate to tumor. Together, our pre-clinical data support an early phase clinical trial of CF10 for treatment of CRC.

Keywords

Colorectal cancer; fluoropyrimidine; cytarabine; replication stress; thymidylate synthase; topoisomerase 1

Introduction

Colorectal cancer (CRC) is a leading cause of cancer-related mortality (1). 5-FU-based regimens were first shown to provide a survival benefit for post-operative adjuvant chemotherapy in 1988 (2), and have been used since to reduce risk for disease recurrence and improve survival. The anti-tumor activity of FPs results primarily from thymidylate synthase (TS) inhibition (3) by the deoxynucleotide FdUMP. However, 5-FU is inefficiently metabolized to FdUMP, and generates relatively higher levels of ribonucleotide metabolites (e.g. FUTP) (4) that cause systemic toxicities as evidenced by reversal of gastrointestinal (GI)-tract (5) and bone marrow toxicities (6) with uridine. 5-FU-related toxicities may be lethal (7), particularly in cancer patients with deficiencies in pyrimidine catabolism due to naturally occurring polymorphisms in *DPYD* (8) and other genes. Risk/benefit considerations limit the applicability of 5-FU-based regimens for patients with stage II colon cancer (9), and dose reduction due to toxicity considerations limit 5-FU efficacy for patients with advanced disease.

Significant research effort continues to focus on enhancing the antineoplastic activity of FPs. Over the past decade we demonstrated that a prototype FP polymer, F10 (10), displayed improved anti-tumor activity relative to 5-FU in multiple pre-clinical models ((11), (12), (13)) through a unique mechanism involving both TS inhibition and Top1 poisoning (10,11). Optimal activity for FP polymers requires uptake of the intact polymer by malignant cells (12), followed by intracellular FdUMP release (14). However, premature F10 degradation likely limits anti-tumor activity. The 2nd generation FP polymer, CF10, includes chemical modifications to both reduce exonucleolytic degradation and enhance activity. In CF10, arabinosyl cytidine (AraC), a nucleoside analog with potent anti-cancer activity (15), and polyethylene glycol (PEG_5) (16), extend the F10 polymer at the 3'- and 5'-termini. AraC is a chain terminating nucleotide analog relatively resistant to exonuclease removal, but removed from DNA via a Tdp1-mediated mechanism (17,18). We predicted that enzymes that degraded single-stranded DNA (ssDNA) would not recognize AraC and, as a result, CF10 would display improved nuclease stability yet eventual AraC release would improve CF10 cytotoxicity to CRC cells relative to F10.

In this study, we demonstrated improved potency for CF10 relative to F10 and 5-FU in multiple CRC cell lines that correlated with reduced thymidine antagonism and improved stability to nuclease degradation, consistent with AraC directly contributing to CF10's cytotoxicity and limiting its nuclease degradation. Mechanistically, both F10 (10) and AraC (19) induce Top1-mediated DNA damage and our studies showed CF10 induced greater Top1cc than F10. CF10 displayed reduced systemic toxicity relative to 5-FU and its anti-tumor activity was established in multiple CRC flank tumor models in mice, which correlated with increased and sustained FdU and FdUMP levels relative to 5-FU. CF10 displayed improved anti-tumor activity relative to 5-FU in an orthotopic tumor model and that correlated with its improved tumor localization relative to a free dye. Our results are consistent with a distinct cytotoxic mechanism for CF10 relative to F10 and 5-FU in CRC cells and distinct pharmacology that may increase FP exposure in GI malignancies resulting in strong anti-tumor activity. Our findings are consistent with CF10 having potential to improve outcomes for CRC patients thru its distinct mechanistic and pharmacological properties.

Materials & Methods

Cell Lines and reagents

HCT116, LS174T, SW480, and T84 CRC cells and HIEC-6 intestinal cells were from ATCC and were cultured using recommended media, validated by short tandem repeat analysis, and regularly confirmed negative for mycoplasma. CF10 and F10 (ST Pharm Co., South Korea) were validated by high-resolution mass spectrometry (Supplementary Fig. S1), and were dissolved in 0.9% sterile saline (Sigma; St. Louis, MO). CF10 and F10 concentrations were determined from A_{260} UV absorbance using extinction co-efficient for ssDNA. Stability of CF10 and F10 to exonuclease digestion with snake venom phosphodiesterase (SVPD) was determined as previously described (20). Clinical-grade 5-FU (50 mg/mL) was purchased from the Baptist Hospital clinical pharmacy. All drugs were filtered using a 0.22 μm filter before injection.

Cell viability and synergy analysis

Cell viability was determined using CellTiter-Glo (Promega, Wisconsin) according to the manufacturer's instructions. To determine drug interactions, cells were treated simultaneously with both agents (e.g. F10+thymidine) in a 5×9 matrix of concentrations chosen to encompass biologically relevant doses, as indicated in the Figures. Combination synergy was determined by Bliss independence analyses via the Combenefit program (21). The difference between the Bliss expectation and the observed growth inhibition of the combination is the Delta.Bliss, and these values were subject to median analysis using Graphpad PRISM.

Clonogenic Assay

1000–5000 cells per well were plated in 6 well plates and treated with serial dilutions of drugs for 10 days with media changed at day 5. Cells were washed with PBS, fixed with 80% methanol, and stained with .05% Crystal Violet (Thermo Fisher Scientific, Waltham, MA). Imaging of colonies was done with the Biorad Chemidoc MP on the Coomassie Blue setting with quantification via the ImageJ (NIH) plugin Colony Area (22), and analyzed using Graphpad PRISM.

Thymidylate synthase activity

TS catalytic assays were performed using well-established procedures (23) with freshly prepared 5,10 methylene tetrahydrofolate in 0.5 M NaOH (Schircks Laboratories, Switzerland), 10 μM dUMP, 200,000 dpm of ^{3}H-dUMP (Moravek Biochemicals), 100 μM 2-mercaptoethanol, and 25 mM KH_2PO_4, pH 7.4. Reactions were quantified by scintillation counting.

DNA fiber assay and high-throughput alkaline comet assay

Cells were treated with either CF10, 5-FU, or DMSO for 16h and analyzed for replication dynamics using DNA fiber assay, as described previously (24). Experiments were performed in triplicate and mean values were presented with statistical significance. For Comet assays, CRC cells were treated with CF10, 5-FU or DMSO for 24 hours. After treatment, cells were trypsinized and analyzed for percent of DNA tail (DNA damage) using 96 well comet chip system as described by the manufacturer (Trevigen, Gaithersburg, MD, USA).

Immunofluorescence

Immunofluorescence detection of pH2AX was performed in drug-treated CRC cells that were fixed and permeabilized using 100% cold methanol and then processed as previously described (24). Top1cc were detected using a primary antibody specific for the cleavage complex (Millipore MABE 1084 and gift of S. Kaufmann) using procedures similar to those previously described (25). Top1cc foci were captured using a Nikon A1R confocal microscope and positive cells were counted via ImageJ with >50 foci considered positive. Top1cc were also detected with the same antibody using a RADAR assay using methods previously described (26).

Western blotting

Proteins were isolated and their differential expressions were analyzed by Western blot as described previously (24). Briefly, cells were lysed in ice-cold cytoskeletal buffer freshly supplemented with protease and phosphatase inhibitors (Roche, Mannheim, Germany). Concentration of the proteins were quantified using Bradford assay (Bio-Rad, USA), and samples were normalized for equal loading. Samples were then heated at 100 °C for 10 minutes in the presence of 6x Laemmli buffer (Boston Bioproducts, Ashland, MA, USA). Proteins were resolved by SDS-PAGE and their expression was analyzed by immunoblotting using specific antibodies.

Colorectal tumor models

Mice were housed and subjected to experiments in accordance with the protocols approved by the Institutional Animal Care and Use Committee (IACUC) at Wake Forest School of Medicine. For flank tumor formation, CRC cells (3×10^6cells) suspended in Matrigel:PBS were injected into the flanks of BALB/c nude mice (for HCT-116 and HT-29) or BALB/c mice (for CT-26) (n=3). Tumor growth and mice health were monitored daily. For orthotopic tumor formation, protocol was followed per Tseng *et al*'s previous study (27). First, flank tumors were formed by subcutaneously injecting HCT116-*luc* cells and monitored until the tumor reached a volume large enough for transplantation, mice were euthanized, and tumor was removed and divided into 2–3 mm pieces. A laparotomy was performed in recipient mice to expose the cecum. A piece of tumor tissue was then attached to the outside of the cecum, the cecum was then returned to the cavity and the abdominal wall closed. Tumor volume and cell progression were monitored using an IVIS Lumina LT Series III and evaluated total photon flux. Pierce D-Luciferin (Thermo Scientific) was injected, i.p. and mice were transferred to the IVIS stage and imaged under 2% isoflurane anesthesia. All images were analyzed using Living Image software using an identical region of interest for each mouse. Two independent studies were performed with identical procedures except in the second study 5-FU (n=9) was dosed 1x/wk at 30 mg/kg (28) rather than 2x/wk every other week at 70 mg/kg (29) because serious GI-tract toxicity was detected in the first study. CF10 was dosed 2x/week every week at 300 mg/kg (n=8 study 1; n=2 in study 2). All drugs or vehicle (0.9% saline; n=8 study 1; n=6 study 2)) were administered by i.p. injection in 200 μL volume. Mice were removed from the study upon weight-loss >20% of initial body weight or when deemed moribund due to tumor burden by veterinary staff.

Tumor localization, blood plasma levels, and blood chemistry

Tumor localization studies used Balb/c nude mice with orthotopic HCT-116-*luc* tumors. A modified CF10 (XF10A) was synthesized in which PEG5 at the 5'-terminus was replaced with a modified PEG5 containing a terminal alkyne. The terminal alkyne of XF10A was coupled to a fluorescent dye (Cy5.5-azide; Lumiprobe) via azide:alkyne Cu^{2+}-catalyzed Click chemistry. The fluorescent CF10 analog (FL_CF10) was characterized by liquid chromatography with diode array detection at 680 nm and 260 nm and by LTQ Orbitrap XL mass spectrometry analysis. 1 nmol of either the Cy 5.5 CF10 conjugate or the free dye were injected via tail vein (n=3 per group). 24h post-injection, mice underwent fluorescence imaging to detect Cy5.5 after which mice were euthanized and liver, tumor and other organs

were imaged ex vivo. Images were analyzed using Living Image software. To determine blood plasma levels of 5-FU, CF10, FdU, FdUMP and other FP metabolites, BALB/c nude mice were injected with CF10 (300 mg/kg) or 5-FU (70 mg/kg) and groups of n=3 at each timepoint (t=0, 30 min, 1h, and 2h post-treatment) mice underwent cardiac puncture under deep isoflurane anesthesia to collect blood samples. Plasma from the collected blood was analyzed by the mass spectrometry and pharmacokinetics shared resource at WFSM to quantify plasma levels of FPs and FP metabolites. Blood chemistry was analyzed in groups of n=5 C57bl/6 mice with no treatment, 5-FU (70 mg/kg) or CF10 (300 mg/kg) 2x/wk. 24h after the second treatment, blood was collected by cardiac puncture under deep isoflurane anesthesia. A portion of the blood was used for complete blood count and plasma from a second portion was used for a complete metabolic panel. Blood testing was performed by IDEXX (Westbrook, ME).

Statistical Analysis

All statistical analyses were conducted using SAS 9.4 or GraphPad Prism. For comparing the tumor growth rates and changes in flux, a mixed model approach was used. Flux values were adjusted for the baseline by dividing observed flux by baseline flux from IVIS imaging. The model included terms for group, time, and group-by-time interactions as fixed effects. The animals were included as random effects to account for the within-animal correlation. Differences in survival times among treatment groups were examined using a Kaplan-Meier analysis and the survival curves were tested for differences using log-rank tests.

Histology Analysis

Tissues from select mice from all treatment groups were removed from animals after undergoing euthanasia by CO_2 asphyxiation and cervical dislocation. In some instances, mice were injected with luciferin ~20 min prior to euthanasia to permit IVIS imaging of extracted tissue. Tumors were weighed after removal and in instances where there was suspicion of possible metastases to liver, lung, or other organs tissue from these organs was removed and if luciferin was administered prior to euthanasia, these tissues were imaged using the IVIS system. All tissues were fixed in 10% neutral buffered formalin for 24h followed by transfer to 70% ethanol. Following routine processing in xylene, tissues were sectioned at 4 μm and stained with Hematoxylin and Eosin and evaluated by light microscopy by a veterinary pathologist.

Results

CF10 displays enhanced potency to CRC cells

First, we evaluated whether CF10 (Fig. 1A; Supplementary Fig. S1) displayed improved stability to exonuclease digestion relative to F10. AraC is not readily recognized by the proofreading activities of DNA polymerases and synthetic DNA extended with AraC may display reduced susceptibility to exonuclease degradation. We treated CF10 and F10 with snake venom phosphodiesterase (SVPD) for 0–16h, and evaluated the relative stabilities of the two FP polymers by gel electrophoresis and mass spectrometry. SVPD is a model nuclease with predominantly 3’-O-exonuclease activity (20). CF10 remained predominantly

intact 1h post-treatment (Fig. 1B) while F10 was degraded to shorter multimers (Fig. 1C). Further, some full length CF10 remained detectable 16h post-treatment (Supplementary Fig. S2).

We next evaluated whether CF10 was more effective than 5-FU and alternative FPs to CRC cells. CF10 was more potent than F10 and much more potent than 5-FU at reducing the clonogenic potential of HCT-116 (Fig. 1D), LS174T (Fig. 1E), T84, and SW480 CRC cells (Supplementary Fig. S3). The potency advantage for CF10 relative to 5-FU far exceeded the 10-fold increased FP content as shown in supplementary Table S1, which includes a summary of IC50 values based on the clonogenic assay results. A CF10 sample was also provided to the NCI developmental therapeutics program for testing in the 60-cell line screen. The NCI data confirmed CF10 (NSC 787877) displayed enhanced growth inhibitory properties relative to F10 (NSC S697912) towards all CRC cell lines in which both agents were tested. CF10 also was more potent than several FP drugs used clinically for CRC treatment including FdU (NSC 27640), 5-FU (NSC 19893), and trifluorothymidine (TFT; NSC 75520). A summary of the mean GI50 values (concentration required to inhibit growth by 50%) for CF10, F10, FdU, 5-FU and TFT from the NCI 60 cell line screen are included in Table S2. CF10 was potent in all CRC cells regardless of the MSI/MSS status or *KRAS* mutation status, which are important factors determining whether CRC patients are treated with FP drugs (30).

CF10 TS/Top1 dual targeting with contribution from AraC

TS is the established target of FP drugs and we previously showed FP polymers were cytotoxic thru dual targeting of TS and Top1 (11). To assess TS inhibition by CF10, we detected TS ternary complex by Western blot, together with the corresponding depletion of unbound TS (Fig. 2A). In HCT-116 cells, CF10 concentrations that inhibited CRC clonogenic survival resulted in TS detection almost exclusively as the ternary complex (Fig. 2A and Supplementary Fig. S4). F10, which has the same FP content as CF10, displayed similar TS ternary complex formation. In contrast, 5-FU, also at 10 nM, did not induce detectable TS ternary complex formation (31), although at much higher 5-FU concentrations (10,000 nM) TS ternary complex formation was evident (Fig. 2A). Similar results were obtained in CF10- and 5-FU-treated LS174T cells (Supplementary Fig. S4). We also evaluated changes in TS catalytic activity using a ^{3}H-release assay (Fig. 2B). CF10 reduced TS catalytic activity at much lower concentrations than 5-FU, and induced a more sustained decrease in TS catalytic activity. Results are consistent with potent TS inhibition being important for CF10's cytotoxicity to CRC cells. To gain further insight into the importance of TS inhibition for CF10 cytotoxicity we co-treated CRC cells with CF10 ± thymidine, and evaluated drug interaction by Bliss synergy analysis. Identical studies were performed with F10 ± thymidine. Thymidine strongly antagonized F10 In both HCT-116 (Fig. 2C) and LS-174T cells (Supplementary Fig. S5) with antagonism ≥ 30 for 14/45 (HCT-116; median = −23±3.6) and 22/45 (LS-174T; median = −26±2.0) of F10+thymidine combinations tested. However, thymidine antagonism was reduced for CF10 relative to F10 with antagonism ≥ 30 for only 5/45 (HCT-116; median −11±2.5) and 17/45 (LS-174T; median −25±1.7) CF10 + thymidine combinations tested. Decreased thymidine antagonism for CF10 was particularly evident in HCT-116 cells that were relatively more sensitive to CF10 compared to F10 (Fig.

1D,E). Our results are consistent with CF10 activating a thymidine-independent cell death mechanism, the extent of which is cell-line dependent.

The enhanced cytotoxicity of CF10 relative to F10 could result from AraC directly contributing to CF10 cytotoxicity. We tested AraC in combination with F10 using Bliss synergy analysis. In HCT-116 cells, AraC was active as a single agent at concentrations that would be released from IC50 values of CF10. Further, the F10+AraC combination was approximately additive with 21/45 of the concentration pairs evaluated displaying combination values of 0±5 relative to the single agents (median −7±2.7; supplementary Fig. S6). LS174T cells also were sensitive to AraC at concentrations that would be released from IC50 values of CF10. However, in LS174T cells the AraC+F10 combination displayed uniform mild antagonism (Supplementary Fig. S6), a result consistent with CF10's reduced potency advantage relative to F10 in LS174T cells (Fig. 1E). To gain further insight into AraC directly contributing to CF10 cytotoxicity, COMPARE analysis (http://dtp.nci.nih.gov; (32)) was conducted to identify mechanistically similar compounds. The compounds with the highest Pearson correlation coefficients (PCC), indicating close mechanistic similarities to CF10, are shown in Supplementary Table S3. CF10 was chosen as the seed and by definition has a Pearson correlation coefficient of 1. The compounds most closely correlated to CF10 included FdU and AraC ranked no. 1 and 3. However, the PCC values were only 0.642 and 0.596 indicating considerable mechanistic differences between CF10 and its constituent nucleosides. Topotecan ranked no. 5, consistent with mechanistic similarities between CF10 and Top1 poisons, as previously established for F10 (10,11). AraC also induces Top1cc formation if stably misincorporated into DNA (19). To determine if CF10 induced Top1cc formation in CRC cells, we performed immunofluorescence (IF) studies with a monoclonal antibody specific for Top1cc (25). CF10 and F10 concentrations that strongly inhibited CRC clonal survival also caused Top1cc (Fig. 2E; Supplementary Fig. S7) with data quantification indicating CF10 was relatively more effective than F10 (Supplementary Fig. S7). Collectively, our studies indicated that AraC may directly contribute to the enhanced cytotoxicity of CF10 relative to F10 in some CRC cells, although AraC's effects on CF10 polymer stability may be more important, particularly in vivo (see below).

CF10 activates the DNA damage response

CF10 strongly inhibits TS (Fig. 2A) and also traps Top1cc at sites of FdU misincorporation into DNA (Fig. 2E), and may generate DNA damage by multiple mechanisms including collisions between advancing replication forks or active transcription complexes with trapped Top1cc (33). Trapped Top1cc at sites of FdU substitution may be particularly deleterious because repair proceeds under thymidine-depleted conditions resulting in FdUTP re-incorporation into DNA during repair, potentially amplifying DNA damage thru futile repair. We analyzed the time-dependent activation of the DNA damage response and demonstrated that 48h post-treatment, CF10 increased mono-ubiquitination of FANCD2 and pChk1 (S317) levels relative to F10 and 5-FU (Fig. 3A; Supplementary Fig. S8), consistent with increased stalled replication forks, but with a delay potentially due to reduced nuclease susceptibility of CF10. DNA fiber analysis confirmed CF10 induced stalled replication forks (Supplementary Fig. S8). CF10 also increased pChk2 (T68), pH2AX, and Rad51 levels

consistent with conversion of stalled forks to DNA double strand breaks (DSBs), which we validated by pH2AX immunofluorescence (Fig. 3B,C) and COMET assays, (Fig. 3D,E).

CF10 is well tolerated and active in vivo.

Our previous studies demonstrated improved anti-tumor activity for F10 relative to 5-FU in multiple pre-clinical models (11–13), even with reduced systemic toxicities. To determine if CF10 differed from 5-FU in selectivity for malignant vs non-malignant cells, we compared CF10 and 5-FU effects in HIEC-6 intestinal cells and HCT-116 CRC cells. Consistent with our clonogenic data (Fig. 1; Supplementary Tables S1 and S2), CF10 was much more than 10-fold more potent than 5-FU to HCT-116 cells; however, CF10 (10^{-6} M) reduced the viability of HIEC-6 cells relatively less than 5-FU (10^{-5} M) at equivalent total FP concentrations (Fig. 4A). We next evaluated the effects of CF10 and 5-FU treatment in vivo to GI-tract tissue in BALB/c mice. Using a previously established dose for 5-FU (29), we observed a single treatment resulted in scattered neutrophils and expanded sub-mucosa consistent with drug-induced inflammation. Conversely, a dose of CF10 that delivered relatively greater FP content had less damaging effects (Fig. 4B). Quantification of crypt and villi lengths in the small intestine revealed CF10 did not significantly decrease average villus length, but 5-FU did (Supplementary Fig. S9). To evaluate potential CF10 toxicity to liver and kidney, we analyzed blood chemistry. Values for alanine aminotransferase (ALT), aspartate aminotransferase (AST), blood urea nitrogen (BUN), and creatinine following CF10 treatment as dosed in efficacy studies (Fig. 5) were similar to control (Supplementary Table S4). While CF10 displayed minimal toxicity to normal tissues, it displayed significant anti-tumor activity at the doses tested in toxicity studies in three CRC flank xenograft models: HCT-116, HT-29, and CT-26 (Fig. 4C-F). In all three models, CF10 displayed significant anti-tumor activity and treatment resulted in no signs of systemic toxicities.

We next evaluated CF10's efficacy in an orthotopic human CRC tumor model using HCT-116-*luc* cells. Mice treated with CF10 (2x/wk; 300 mg/kg) displayed stable weights and on average gained weight during a substantial portion of the study with treatment extending to 8 weeks (Fig. 5A). Mice treated with CF10 also remained active throughout the study with no signs of drug-related toxicity. Analysis of tumor growth rates showed the CF10 group had significantly reduced tumor growth than either 5-FU or vehicle ($p=0.014$). A summary of tumor growth rates for the three treatment groups is included in Fig. 5B, and representative IVIS images and a summary of the week 5 flux values is presented in Fig. 5D,E. We examined whether differences in tumor growth among groups were more pronounced in the early (first 3-weeks) or later (3–6 week) time periods, but did not find evidence of this occurring. CF10 treatment also resulted in markedly prolonged survival in the HCT-116-luc orthotopic model (median 84.5 days) relative to vehicle control (median 33 days). When we examined survival times among groups we found a highly significant difference based on the Log-Rank test (chi-square 19.8, 2 degrees of freedom $p<0.0001$) – with the CF10 animals having much longer survival (median 84.5 days) than control or 5-FU (33 days and 32 days, respectively). Mice were removed from the study upon excessive weight loss or when deemed moribund due to tumor burden by Veterinary staff. A Kaplan-Meier presentation of the survival data is displayed in Fig. 5C. CF10 also trended towards improved survival relative to F10 (Supplementary Fig. S10). Our results demonstrate CF10

increases survival in an orthotopic model of HCT-116-*luc* CRC, while 5-FU had no significant effect on survival in this model. To determine if the high tumor burden for mice in the 5-FU and vehicle treatment groups was associated with metastases, select mice that underwent euthanasia from morbidities associated with large tumor burden (i.e. lethargy, hunched posture) at week 5 were subjected to autopsy following euthanasia. Liver, lung, kidney and other tissues were inspected for gross morphological features consistent with metastases. Putative metastatic tissue was evident in 2/4 of 5-FU-treated mice and in 3/5 of the vehicle-treated group. One otherwise viable CF10-treated mouse was euthanized at week 8 and extensive analysis of liver tissue from autopsy revealed no signs of liver metastasis (Supplementary Fig. S11). The data indicate the HCT-116 orthotopic tumor model develops spontaneous metastases and are consistent with CF10 significantly reducing tumor burden and potentially reducing metastatic progression.

CF10 in vivo metabolism and targeting

To further investigate the pharmacological basis for CF10's improved anti-tumor activity relative to 5-FU in the orthotopic tumor model, we quantified FP metabolites from mouse plasma following intra-venous CF10 or 5-FU injection (Fig. 6A), and evaluated CF10's biodistribution using a fluorescent conjugate (Fig. 6B; Supplementary Fig. S12). Consistent with previous reports of 5-FU's rapid plasma clearance, 5-FU plasma concentration rapidly decreased to <2% of initial values 30 min post-treatment and was undetected at longer timepoints. Previous studies with phosphodiester ODNs of similar chemical composition as CF10 showed rapid plasma clearance via active transport into parenchymal and non-parenchymal liver tissue (34) followed by MRP2-dependent biliary secretion (35). We detected CF10 (supplementary Fig S13A) and shorter multimers (CF9, CF8, etc.; supplementary Fig S13B) immediately following injection, but not at later timepoints. However, FdUMP and FdU plasma concentrations were sustained over >1h following CF10 injection (Fig. 6), while these were barely detectable following 5-FU treatment (Fig. 6). To gain further insight into CF10's biodistribution, we prepared a fluorescent conjugate of CF10 and performed IVIS imaging following i.v. injection in which HCT-116-luc orthotopic CRC tumors were previously established (Fig. 6B). 24h Post-injection, FL_CF10 differed from the free dye in biodistribution (Fig. 6B). To further analyze CF10's biodistribution, we euthanized the mice, rapidly extracted tissues, and performed ex vivo imaging of tumor and liver from all mice (Fig. 6B). Strong tumor localization was evident for FL_CF10 while the free dye localized primarily in liver. Data quantification demonstrated an increased tumor/liver ratio for FL_CF10 relative to free-dye (Fig. 6B). Our results are consistent with CF10 localizing to orthotopic colon tumors following i.v. injection, which may occur in part thru hepatobiliary clearance and contribute to CF10's strong activity towards orthotopic colon tumors.

Discussion

Fluoropyrimidine drugs (FPs) remain central to CRC treatment (3) and 5-FU, the most widely used FP, is used to treat >2 million cancer patients each year (36). Despite decades of optimizing its schedule and modulating activity by co-treatment with leucovorin and other agents (37,38), the narrow therapeutic index of 5-FU remains a major obstacle to improving

outcomes with FP drugs, particularly for mCRC patients (30,39). In this study, we highlighted the improved activity of a novel 2nd generation FP polymer, CF10 relative to both 5-FU and F10, a prototype FP polymer with established anti-cancer activity in multiple pre-clinical models . We demonstrated that the chemical modifications that differentiate CF10 from F10, AraC extension and PEG_5 conjugation (Fig. 1A; Supplementary Fig. 1), improved both CF10's stability to enzymatic degradation (Fig 1B,C) and its potency relative to FP drugs used to treat CRC, including 5-FU (Fig. 1D,E), FdU, and TFT (Supplementary Tables S1 and S2). Importantly, CF10 displayed strong anti-tumor activity, which we also demonstrated in vivo with flank (Fig. 4) and orthotopic tumor xenografts (Fig. 5).

CF10 was chemically modified from the prototype FP polymer F10 by extension at the termini with AraC and PEG_5. AraC is a chain terminating nucleoside analog that is not readily removed by proofreading activities of DNA polymerases and we reasoned that extending the 3'-terminus of F10 would decrease susceptibility to enzymatic hydrolysis and potentially enhance anti-tumor activity since AraC is cytotoxic to malignant cells. Consistent with this goal, our findings established that CF10 is stabilized to exonuclease degradation (Fig. 1B,C) and more potent than F10 and much more potent than 5-FU in multiple CRC cell lines (Supplementary Tables S1 and S2). Our data also support a direct contribution of AraC release to CF10 cytotoxicity as concentrations of AraC that would be released from effective concentrations of CF10 displayed single agent activity in CRC cells (Supplementary Fig. S6). Further, the increased potency of CF10 relative to F10 correlates with decreased thymidine antagonism (Fig 2 C,D) consistent with a non-FP component to cytotoxicity. Hence, CF10's cytotoxicity advantage relative to F10 results in part, from AraC both decreasing susceptibility to nuclease degradation and a direct cytotoxic component resulting from AraC release.

Mechanistically, CF10's substantial potency advantage relative to 5-FU in CRC cells is associated with increased replication stress. Malignant cells experience high levels of replication stress (40), and drugs enhancing replication stress display strong anti-cancer activity (41,42). We demonstrated that CF10, but not 5-FU, significantly reduced replication fork velocity and increased terminal replication forks (Supplementary Fig. S8), consistent with increased replication stress. The causes of replication stress are diverse, and include deoxynucleotide depletion and imbalance that result from TS inhibition and Top1cc formation. CF10 strongly inhibits TS as evidenced by TS ternary complex formation (Fig. 2A). A source of CF10-induced replication stress in addition to thymidine depletion is Top1cc formation. Top1 is the sole target for topotecan, and Top1 is also poisoned by FdU (10) and AraC (19) misincorporation into DNA. In these studies, we demonstrated using IF that CF10 induced significantly greater Top1cc in CRC cells than F10 (Fig. 2E).

5-FU causes serious GI- and hematological toxicities in many patients, particularly patients deficient in pyrimidine catabolism due to polymorphisms in DPYD (8). In the present studies, 5-FU was administered at a previously established maximum tolerated dose (70 mg/kg, 2x/wk every other week; (29)), and even a single dose at this concentration resulted in an inflammatory response to the GI-tract as evidenced by increased neutrophils and edema (Fig. 4B). Clinically, both the GI- and hematological toxicities of 5-FU are reversed with uridine consistent with an RNA-directed origin. FP polymers, in principle, are

converted to deoxyribonucleotides, which we confirmed both by enzymatic hydrolysis ex vivo (Fig. 1B,C; Supplementary Fig. S2) and by analyzing plasma metabolite levels in vivo (Fig. 6A; Supplementary Fig. S13). Because of reduced RNA mediated effects, CF10 causes less GI tract damage than equivalent 5-FU concentrations (Supplementary Fig. S9) enabling higher CF10 doses to be tolerated. Evaluation of blood chemistry at these higher doses did not reveal evidence for kidney or liver toxicity (supplementary Table S4), and observational studies revealed these higher doses to be tolerated even with extensive, multi-week treatment.

The ability to dose CF10 at higher levels than 5-FU without causing serious systemic toxicities likely contributes to CF10's improved anti-tumor activity relative to 5FU, but other factors are important. CF10 treatment resulted in increased FdU and FdUMP plasma levels relative to 5-FU (Fig. 6A), and these metabolites are important for anti-tumor activity. Further, with CF10 we observed greater selectivity for malignant (i.e. HCT-116) relative to non-malignant cells (i.e. HIEC-6) compared to 5-FU (Fig. 4A), which could result from increased reliance of malignant cells on de novo thymidine biosynthesis. Finally, a CF10 fluorescent conjugate displayed an altered biodistribution relative to the unconjugated dye and strong tumor uptake was evident for the conjugate (Fig. 6B). Phosphodiester oligonucleotides of similar chemical composition as CF10 undergo receptor-mediated uptake in liver (34) followed by MRP2-mediated biliary excretion (35). Similar routing of CF10 could be responsible for the improved tumor localization of the fluorescent CF10 conjugate relative to the free dye. Further, hepatobiliary routing of CF10 could result in increased FP exposure in the GI-tract contributing to improved anti-tumor activity (Fig. 5). Unlike purine metabolites that are degraded to uric acid before absorption, pyrimidines remain intact, and are readily absorbed from the intestine (43). Interestingly, the HCT-116 orthotopic tumor model used displayed evidence of metastatic progression for the vehicle and 5-FU treatment groups (Supplementary Fig. S11A,B). However, while animal numbers were limited, our data suggest CF10 treatment may impede metastatic progression (Supplementary Fig. S11C), although further studies are needed to conclusively test this. CF10 also displayed a trend towards improved survival relative to F10 (Supplementary Fig. S10), consistent with its improved potency relative to F10 towards CRC cells in cell culture.

Overall, our findings underscore that CF10 is more potent than F10 or current FP drugs and that the improved activity of CF10 relative to F10 results from AraC's effects contributing to both polymer stability and cytotoxicity. The AraC component of CF10 likely is responsible for reduced thymidine antagonism relative to F10 (Fig. 2C,D), as well as increased potency to CRC cells (Supplementary Tables S2 and S3). CF10 is well-tolerated in vivo (Fig. 4B) and increased tolerability together with enhanced selectivity to malignant cells (Fig. 4A), improved conversion to deoxynucleotide FP metabolites (Fig. 6A), and altered biodistribution (Fig. 6B), all likely contribute to CF10's improved potency relative to 5-FU toward orthotopic CRC tumors (Fig. 5). Our findings support advanced pre-clinical testing of CF10 and initiation of clinical studies in CRC and other aggressive tumor types.

Supplementary Material

Refer to Web version on PubMed Central for supplementary material.

Acknowledgements

This study was performed with grant support from 1R21 CA218933 (to W.H. Gmeiner), 1R01CA212600–01 (J.R. Brody) and R01 CA212600 (K. Palle). This work was also supported, in part, by a National Cancer Institute of the National Institutes of Health under a Cancer Center Support Grant P30CA012197 (WFBHCCC) and P30CA056036 SKCC Core Grant (Thomas Jefferson University). The authors wish to acknowledge the support of the Wake Forest Baptist Comprehensive Cancer Center Biostatistics Shared Resource, Cell and Viral Vector Shared Resource, and the Proteomics and Metabolomics Shared Resource and the WFU mass Spectrometry facility. The authors' are grateful for technical assistance from B. Kuhlman, T. Bor, M. Manandhar, M. Regan, C. Tracy, E. Routh, S. Rideout.

Financial support: NIH-NCI R21 CA218933 (WG), NIH-NCI P30 CA012197 (BP), 1R01CA212600–01 (JRB), P30CA056036 (JRB), Weitlauf Endowment Funds (KP), R01CA219187 (KP).

References

1. Arnold M, Sierra MS, Laversanne M, Soerjomataram I, Jemal A, Bray F. Global patterns and trends in colorectal cancer incidence and mortality. Gut 2017;66:683–91. [PubMed: 26818619]
2. Wolmark N, Fisher B, Rockette H, Redmond C, Wickerham DL, Fisher ER, et al. Postoperative adjuvant chemotherapy or BCG for colon cancer: results from NSABP protocol C-01. J Natl Cancer Inst 1988;80:30–6. [PubMed: 3276901]
3. Wilson PM, Danenberg PV, Johnston PG, Lenz HJ, Ladner RD. Standing the test of time: targeting thymidylate biosynthesis in cancer therapy. Nat Rev Clin Oncol 2014;11:282–98 [PubMed: 24732946]
4. Noordhuis P, Holwerda U, Van der Wilt CL, Van Groeningen CJ, Smid K, Meijer S, et al. 5-Fluorouracil incorporation into RNA and DNA in relation to thymidylate synthase inhibition of human colorectal cancers. Ann Oncol 2004;15:1025–32. [PubMed: 15205195]
5. Pritchard DM, Watson AJ, Potten CS, Jackman AL, Hickman JA. Inhibition by uridine but not thymidine of p53-dependent intestinal apoptosis initiated by 5-fluorouracil: evidence for the involvement of RNA perturbation. Proc Natl Acad Sci U S A 1997;94:1795–9. [PubMed: 9050858]
6. van Groeningen CJ, Peters GJ, Leyva A, Laurensse E, Pinedo HM. Reversal of 5-fluorouracil-induced myelosuppression by prolonged administration of high-dose uridine. J Natl Cancer Inst 1989;81:157–62. [PubMed: 2909757]
7. Ma WW, Saif MW, El-Rayes BF, Fakih MG, Cartwright TH, Posey JA, et al. Emergency use of uridine triacetate for the prevention and treatment of life-threatening 5-fluorouracil and capecitabine toxicity. Cancer 2017;123:345–56. [PubMed: 27622829]
8. Diasio RB. The role of dihydropyrimidine dehydrogenase (DPD) modulation in 5-FU pharmacology. Oncology (Williston Park) 1998;12:23–7.
9. Varghese A. Chemotherapy for Stage II Colon Cancer. Clin Colon Rectal Surg 2015;28:256–61 [PubMed: 26648796]
10. Liao ZY, Sordet O, Zhang HL, Kohlhagen G, Antony S, Gmeiner WH, et al. A novel polypyrimidine antitumor agent FdUMP[10] induces thymineless death with topoisomerase I-DNA complexes. Cancer Res 2005;65:4844–51. [PubMed: 15930305]
11. Pardee TS, Gomes E, Jennings-Gee J, Caudell D, Gmeiner WH. Unique dual targeting of thymidylate synthase and topoisomerase1 by FdUMP[10] results in high efficacy against AML and low toxicity. Blood 2012;119:3561–70. [PubMed: 22362039]
12. Pardee TS, Stadelman K, Jennings-Gee J, Caudell DL, Gmeiner WH. The poison oligonucleotide F10 is highly effective against acute lymphoblastic leukemia while sparing normal hematopoietic cells. Oncotarget 2014;5:4170–9. [PubMed: 24961587]
13. Gmeiner WH, Lema-Tome C, Gibo D, Jennings-Gee J, Milligan C, Debinski W. Selective anti-tumor activity of the novel fluoropyrimidine polymer F10 towards G48a orthotopic GBM tumors. J Neurooncol 2014;116:447–54. [PubMed: 24346635]
14. Bijnsdorp IV, Comijn EM, Padron JM, Gmeiner WH, Peters GJ. Mechanisms of action of FdUMP[10]: metabolite activation and thymidylate synthase inhibition. Oncol Rep 2007;18:287–91. [PubMed: 17549381]

15. Grem JL, Geoffroy F, Politi PM, Cuddy DP, Ross DD, Nguyen D, et al. Determinants of sensitivity to 1-beta-D-arabinofuranosylcytosine in HCT 116 and NCI-H630 human colon carcinoma cells. Mol Pharmacol 1995;48:305–15. [PubMed: 7651364]
16. Shokrzadeh N, Winkler AM, Dirin M, Winkler J. Oligonucleotides conjugated with short chemically defined polyethylene glycol chains are efficient antisense agents. Bioorg Med Chem Lett 2014;24:5758–61. [PubMed: 25453815]
17. Huang SY, Murai J, Dalla Rosa I, Dexheimer TS, Naumova A, Gmeiner WH, et al. TDP1 repairs nuclear and mitochondrial DNA damage induced by chain-terminating anticancer and antiviral nucleoside analogs. Nucleic Acids Res 2013;41:7793–803 [PubMed: 23775789]
18. Gmeiner WH, Skradis A, Pon RT, Liu J. Cytarabine-induced destabilization of a model Okazaki fragment. Nucleic Acids Res 1998;26:2359–65. [PubMed: 9580686]
19. Pourquier P, Takebayashi Y, Urasaki Y, Gioffre C, Kohlhagen G, Pommier Y. Induction of topoisomerase I cleavage complexes by 1-beta -D-arabinofuranosylcytosine (ara-C) in vitro and in ara-C-treated cells. Proc Natl Acad Sci U S A 2000;97:1885–90. [PubMed: 10677551]
20. Bowman KJ, Pla RL, Guichard Y, Farmer PB, Jones GD. Evaluation of phosphodiesterase I-based protocols for the detection of multiply damaged sites in DNA: the detection of abasic, oxidative and alkylative tandem damage in DNA oligonucleotides. Nucleic Acids Res 2001;29:E101. [PubMed: 11600720]
21. Di Veroli GY, Fornari C, Wang D, Mollard S, Bramhall JL, Richards FM, et al. Combenefit: an interactive platform for the analysis and visualization of drug combinations. Bioinformatics 2016;32:2866–8. [PubMed: 27153664]
22. Guzman C, Bagga M, Kaur A, Westermarck J, Abankwa D. ColonyArea: an ImageJ plugin to automatically quantify colony formation in clonogenic assays. PLoS One 2014;9:e92444 [PubMed: 24647355]
23. Gmeiner WH, Trump E, Wei C. Enhanced DNA-directed effects of FdUMP[10] compared to 5FU. Nucleosides Nucleotides Nucleic Acids 2004;23:401–10. [PubMed: 15043163]
24. Mani C, Pai S, Papke CM, Palle K, Gmeiner WH. Thymineless Death by the Fluoropyrimidine Polymer F10 Involves Replication Fork Collapse and Is Enhanced by Chk1 Inhibition. Neoplasia 2018;20:1236–45. [PubMed: 30439567]
25. Patel AG, Flatten KS, Peterson KL, Beito TG, Schneider PA, Perkins AL, et al. Immunodetection of human topoisomerase I-DNA covalent complexes. Nucleic Acids Res 2016;44:2816–26. [PubMed: 26917015]
26. Kiianitsa K, Maizels N. A rapid and sensitive assay for DNA-protein covalent complexes in living cells. Nucleic Acids Res 2013;41:e104. [PubMed: 23519618]
27. Tseng W, Leong X, Engleman E. Orthotopic mouse model of colorectal cancer. J Vis Exp 2007:484. [PubMed: 18989400]
28. Rick FG, Buchholz S, Schally AV, Szalontay L, Krishan A, Datz C, et al. Combination of gastrin-releasing peptide antagonist with cytotoxic agents produces synergistic inhibition of growth of human experimental colon cancers. Cell Cycle 2012;11:2518–25. [PubMed: 22751419]
29. Guo J, Zhou AW, Fu YC, Verma UN, Tripathy D, Frenkel EP, et al. Efficacy of sequential treatment of HCT116 colon cancer monolayers and xenografts with docetaxel, flavopiridol, and 5-fluorouracil. Acta Pharmacol Sin 2006;27:1375–81. [PubMed: 17007746]
30. Punt CJ, Koopman M, Vermeulen L. From tumour heterogeneity to advances in precision treatment of colorectal cancer. Nat Rev Clin Oncol 2016; 14:235–246. [PubMed: 27922044]
31. Brody JR, Gallmeier E, Yoshimura K, Hucl T, Kulesza P, Canto MI, et al. A proposed clinical test for monitoring fluoropyrimidine therapy: detection and stability of thymidylate synthase ternary complexes. Cancer Biol Ther 2006;5:923–7. [PubMed: 16855390]
32. Paull KD, Shoemaker RH, Hodes L, Monks A, Scudiero DA, Rubinstein L, et al. Display and analysis of patterns of differential activity of drugs against human tumor cell lines: development of mean graph and COMPARE algorithm. J Natl Cancer Inst 1989;81:1088–92. [PubMed: 2738938]
33. Gmeiner WH. Entrapment of DNA topoisomerase-DNA complexes by nucleotide/nucleoside analogs. Cancer Drug Resist 2019;2:994–1001. [PubMed: 31930190]

34. Biessen EA, Vietsch H, Kuiper J, Bijsterbosch MK, Berkel TJ. Liver uptake of phosphodiester oligodeoxynucleotides is mediated by scavenger receptors. Mol Pharmacol 1998;53:262–9. [PubMed: 9463484]

35. Lischka K, Starke D, Failing K, Herling A, Kramer W, Petzinger E. Hepatobiliary elimination of bile acid-modified oligodeoxynucleotides in Wistar and TR- rats: evidence for mrp2 as carrier for oligodeoxynucleotides. Biochem Pharmacol 2003;66:565–77. [PubMed: 12906921]

36. An Q, Robins P, Lindahl T, Barnes DE. 5-Fluorouracil incorporated into DNA is excised by the Smug1 DNA glycosylase to reduce drug cytotoxicity. Cancer Res 2007;67:940–5. [PubMed: 17283124]

37. Thirion P, Piedbois P, Buyse M, O'Dwyer PJ, Cunningham D, Man A, et al. Alpha-interferon does not increase the efficacy of 5-fluorouracil in advanced colorectal cancer. Br J Cancer 2001;84:611–20. [PubMed: 11237380]

38. Grem JL. Mechanisms of Action and Modulation of Fluorouracil. Semin Radiat Oncol 1997;7:249–59. [PubMed: 10717222]

39. Wang J, Li S, Liu Y, Zhang C, Li H, Lai B. Metastatic patterns and survival outcomes in patients with stage IV colon cancer: A population-based analysis. Cancer Med 2020;9:361–73 [PubMed: 31693304]

40. Gaillard H, Garcia-Muse T, Aguilera A. Replication stress and cancer. Nat Rev Cancer 2015;15:276–89. [PubMed: 25907220]

41. Ubhi T, Brown GW. Exploiting DNA Replication Stress for Cancer Treatment. Cancer Res 2019;79:1730–9. [PubMed: 30967400]

42. Puigvert JC, Sanjiv K, Helleday T. Targeting DNA repair, DNA metabolism and replication stress as anti-cancer strategies. FEBS J 2016;283:232–45. [PubMed: 26507796]

43. Loffler M, Fairbanks LD, Zameitat E, Marinaki AM, Simmonds HA. Pyrimidine pathways in health and disease. Trends Mol Med 2005;11:430–7. [PubMed: 16098809]

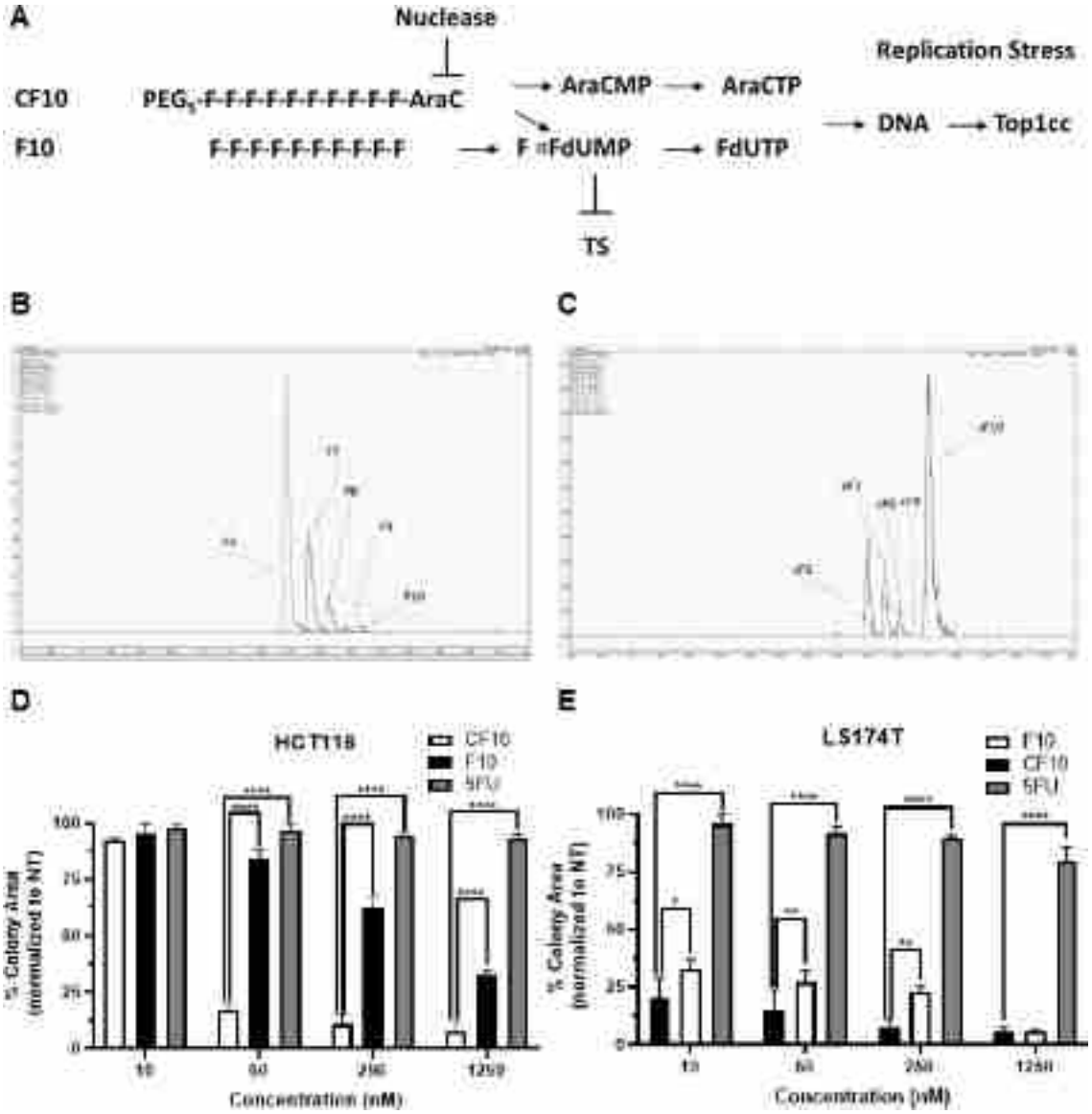

Figure 1.

Chemical modification to CF10 increases stability to exonuclease degradation and improves potency toward CRC cells. **A,** Scheme depicting CF10's cytotoxic mechanism. AraC extension of the FP polymer reduces nuclease digestion but eventual release of FdUMP inhibits thymidylate synthase and incorporation of FdUTP and AraCTP into DNA causes Top1cc and replication stress. **B,C,** snake venom phosphodiesterase hydrolysis of **B**, CF10 and **C**, F10 1h post-treatment. **D,E**, Summary of clonogenic assays evaluating CF10, F10, and 5-FU in **D**, HCT-116 and **E**, LS174T cells.

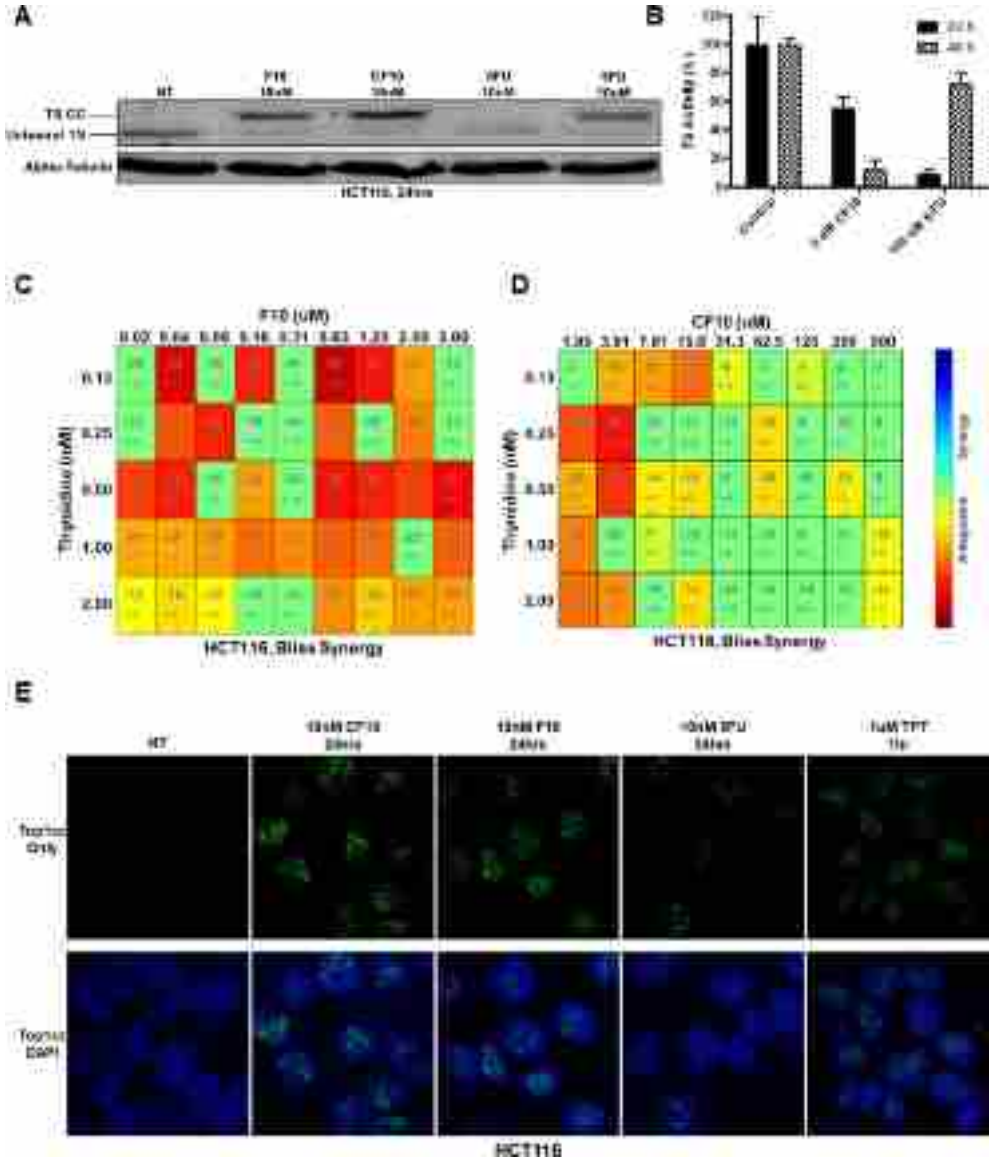

Figure 2.

CF10 strongly inhibits TS but is less sensitive to thymidine antagonism than F10. **A**, Western blot detecting TS ternary complex (TS CC) in HCT-116 cells 24h post-treatment with the indicated treatment. **B**, TS activity assay showing reduced TS catalytic activity following CF10 treatment. **C,D** Bliss synergy analysis showing deviation from expected activity based on strict additivity for the indicated concentrations of thymidine and **C**, F10 and **D**, CF10. **E**, Immunofluorescence data showing Top1cc in HCT-116 cells following the indicated treatments.

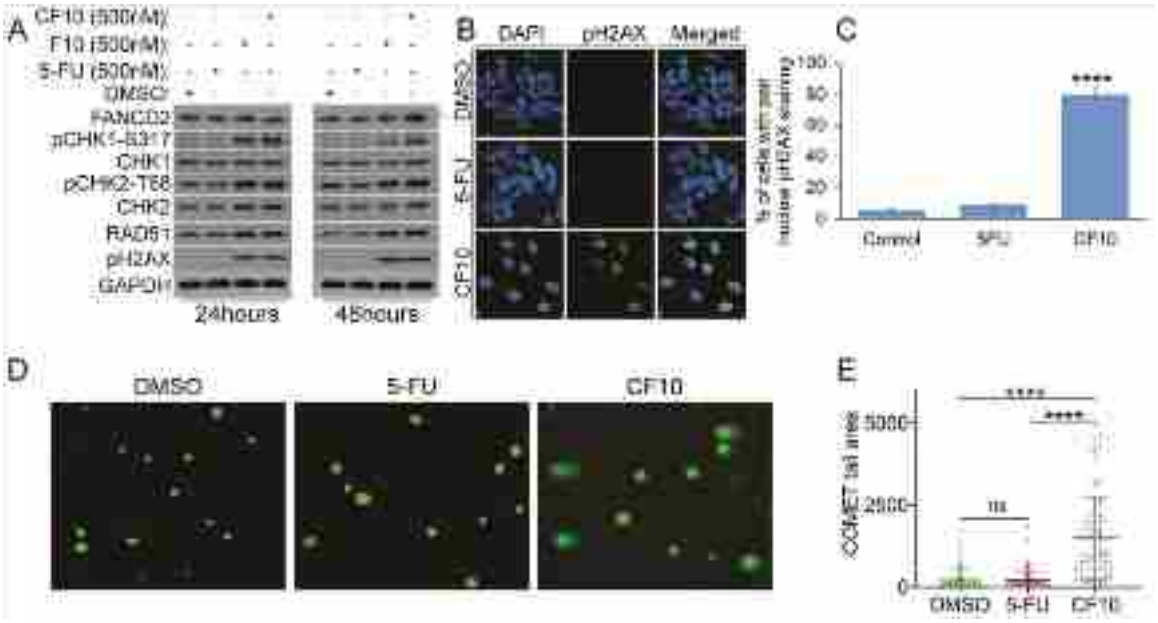

Figure 3.

CF10 stimulates prolonged activation of the DNA damage response and induces formation of DNA double strand breaks (DSBs). **A**, Western blot for markers of stalled replication forks (FANCD2, pChk1-S317) and DNA DSBs (pChk2-T68, Rad51, pH2AX) 24h or 48h with the indicated treatment in HCT-116 cells. **B,** Immunofluorescence imaging of pH2AX in HCT-116 cells following treatment with CF10 or 5-FU at 500 nM. **C**, Quantification of immunofluorescence data in **B**. **D**, Results of alkaline COMET assay following treatment with CF10 or 5-FU at 500 nM. **E**, Quantification of data in **D**.

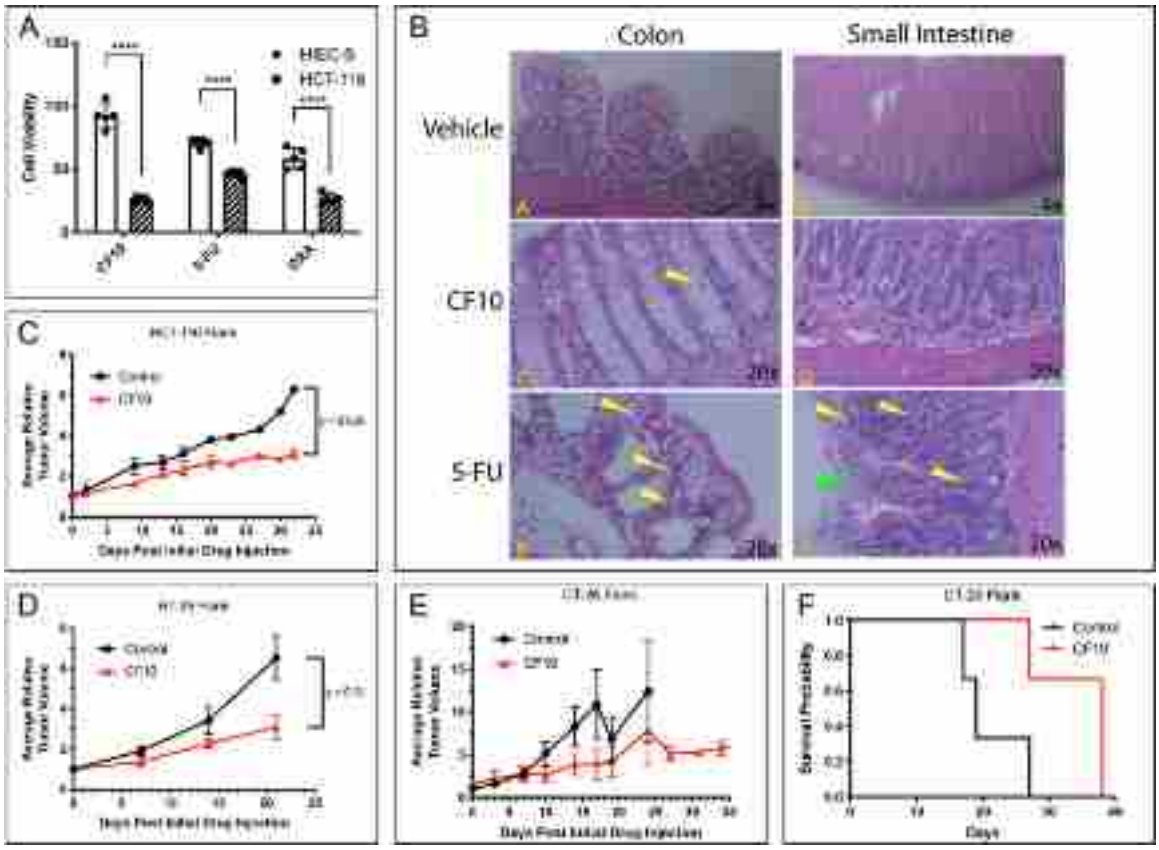

Figure 4.

CF10 displays reduced toxicity to non-malignant cells and tissue and anti-tumor activity in CRC flank tumor models. **A**, Effects of CF10 (10–6M), 5-FU (10–5M), and oxaliplatin (10–5M) in HIEC-6 intestinal cells and HCT-116 CRC cells with 72h treatment and viability determined using CellTiter-Glo (Promega). The doses of CF10 and 5-FU have equivalent FP content. **B**, H&E stained sections from BALB/c mice 24h after treatment with (A,B) – vehicle – (4x), note normal colon and small intestine epithelium. (C,D) – CF10 300 mg/kg (20x). Minimal to scant nuclear debris in colonic epithelium (yellow arrow) and small intestine crypts have scattered to minimal nuclear debris (apoptosis). (E.F) 5-FU 70 mg/kg (20x) Colon with scattered neutrophils (yellow arrows) and expanded sub-mucosa (green arrow; e.g. edema). Small intestine with increased crypt apoptosis and scattered neutrophils. **C-E**, Growth rates for HCT-116 (C), HT-29 (D), and CT-26 (E) flank tumors showing CF10 (300 mg/kg; 2x/wk) significantly reduced tumor growth. **F**, CF10 increased survival in a CT-26 flank tumor model.

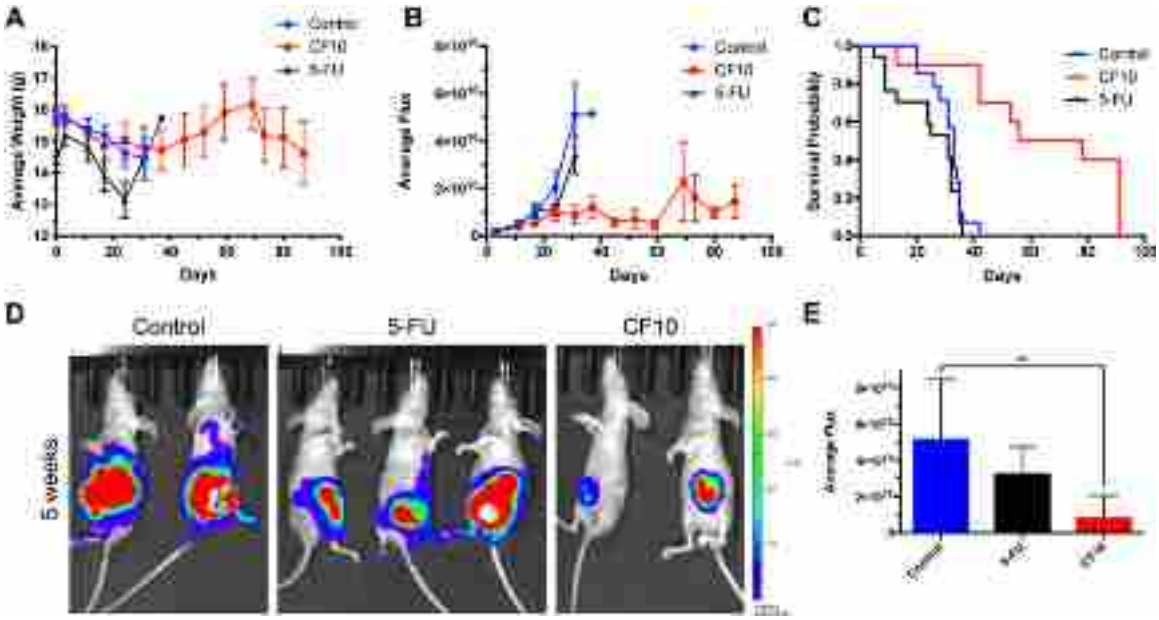

Figure 5.

CF10 treatment (300 mg/kg 2x/wk for 8 weeks) inhibits tumor growth in an orthotopic model and provides a significant survival advantage relative to vehicle and 5-FU treatment (70 mg/kg 2x/wk qow). **A**, Graph of mouse weights for control (blue), CF10 (red), and 5-FU (black) treatment groups. **B**, Graph of flux from HCT-116-luc orthotopic xenografts. Differences in the rate of change in flux among the groups were not significant during the first three weeks of treatment however the groups then diverged, and flux rate was significantly lower in CF10 treated mice (red) relative to vehicle (blue) or 5-FU (black) treated mice. **C**, Kaplan-Meier plot showing a survival advantage for CF10 (red) relative to vehicle (blue) and 5-FU (black). Differences in survival were significant based on Log-Rank test (chi-square 19.8, 2 degrees of freedom $p<0.0001$). **D**, Representative IVIS images for mice after 5 weeks of the indicated treatment. **E**, Quantification of IVIS images from (**D**).

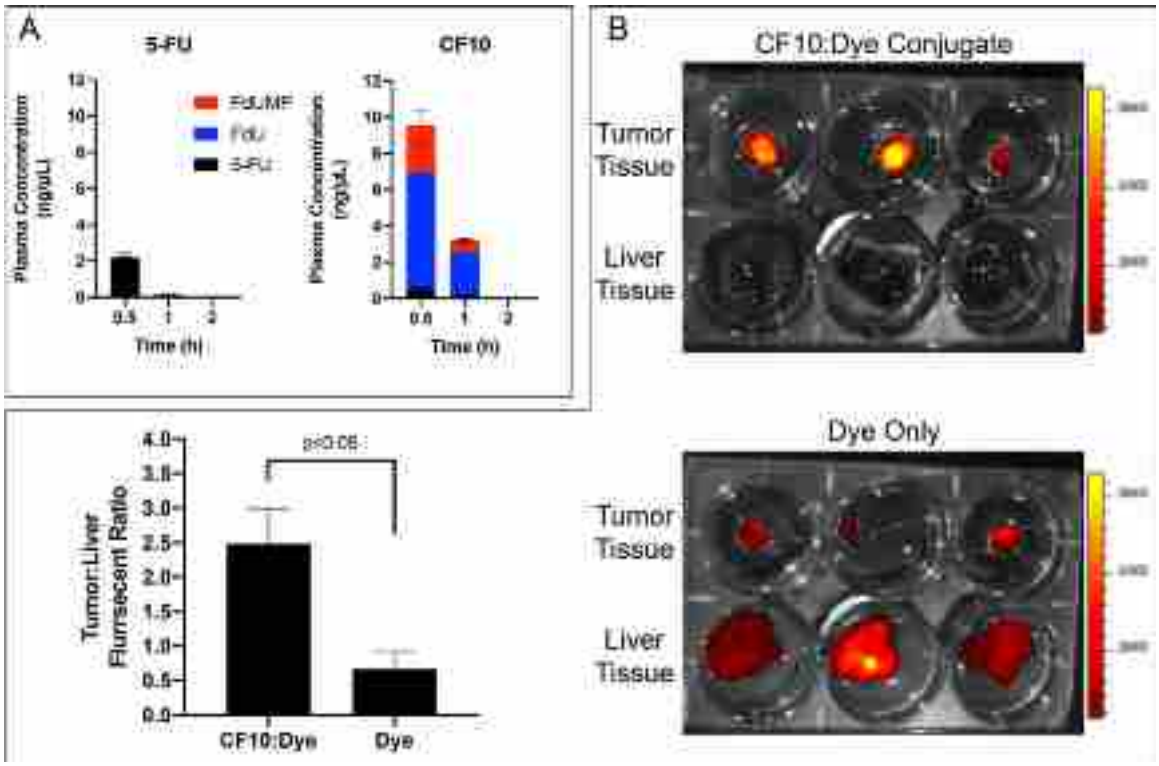

Figure 6.

CF10 results in sustained plasma concentrations of FP deoxynucleosides (FdUMP and FdU) and localizes to orthotopic CRC tumors. **A**, Plasma concentrations of 5-FU (black), FdU (blue), and FdUMP (red) determined by LC/MS following tail vein injection of 5-FU (left) and CF10 (right). **B**, A fluorescent conjugate of CF10 localizes to orthotopic colon tumors, in vivo. Mice with pre-established orthotopic HCT-116 tumors were injected with either FL_CF10 or free dye and underwent near-infrared imaging 24h post-injection. Ex vivo imaging of tumor (top row) and liver (bottom row) from mice treated with FL_CF10 (top) or free dye (bottom). (E) Quantification of imaging data is shown in bottom left.